CWI

A thermostat closure for point vortices

S. Dubinkina, J.E. Frank, B.J. Leimkuhler

MAS-E0909

Centrum Wiskunde & Informatica

Centrum Wiskunde & Informatica (CWI) is the national research institute for Mathematics and Computer Science. It is sponsored by the Netherlands Organisation for Scientific Research (NWO).
CWI is a founding member of ERCIM, the European Research Consortium for Informatics and Mathematics.

CWI's research has a theme-oriented structure and is grouped into four clusters. Listed below are the names of the clusters and in parentheses their acronyms.

Probability, Networks and Algorithms (PNA)

Software Engineering (SEN)

Modelling, Analysis and Simulation (MAS)

Information Systems (INS)

P.O. Box 94079, 1090 GB Amsterdam (NL)
Science Park 123, 1098 XG Amsterdam (NL)
Telephone +31 20 592 9333
Telefax +31 20 592 4199

ISSN 1386-3703

A THERMOSTAT CLOSURE FOR POINT VORTICES

SVETLANA DUBINKINA*, JASON FRANK †, AND BEN LEIMKUHLER‡

Abstract. Using the point vortex flow on a disc as a prototype, we present a closure for incompressible ideal fluid flow in the form of a generalized thermostating device. The thermostat can model either an infinite or finite reservoir. The thermostat variables are stochastically forced. Numerical experiments are in excellent agreement with the two-scale simulations of Bühler (*Phys. Fluids*, 2002).

Key words. thermostat methods, point vortex fluid, closure models, geophysical fluid dynamics

AMS subject classifications. 65M99, 65P10, 86A10, 82B99

1. Background. Inviscid fluid models are natural in a number of application areas, such as atmosphere and ocean science, where the Reynolds numbers are so large as to be effectively infinite. These flows are characterized by conservation of total energy, the cascade of vorticity to ever finer scales, and sensitive dependence on initial conditions [15].

For the numerical simulation of such flows, the lack of a viscous diffusion length scale presents the challenge that due to the vorticity cascade, any direct discretization of the equations of motion must eventually become underresolved, as vorticity is transported to scales below the grid resolution. It therefore becomes necessary to close the numerical model by some means. Any finite numerical discretization implies a closure of some kind, whether explicitly modeled or implied by the discretization [4].

The most common approach is the introduction of artificial viscosity, either through modification of the fluid equations to include (hyper-)viscosity, or through the use of stabilized discretizations, for which the viscous terms appear in a modified equation analysis [6]. In either case the viscous length scale must be on the order of the grid resolution to be effective. One disadvantage with a viscous closure model is that it precludes an upscale cascade of vorticity, thereby suppressing hydrodynamic instabilities in geophysical flows, especially in three dimensions. Alternatively, methods can be constructed that preserve the discrete total energy exactly. However, this is achieved via a nonphysical re-injection of the energy from sub-gridscale vorticity at the large scales [12].

A proper closure model should distinguish between resolved and unresolved scales and account for the exchange between these. In this paper we consider a simple two-scale point vortex flow, consisting of a small number of vortices with large circulation and a very large number of vortices with a much smaller circulation. We seek a simplified computational model for the aggregate behavior of the small-scale point vortices.

The situation is reminiscent of statistical mechanics in the canonical ensemble,

*Centrum Wiskunde & Informatica, P.O. Box 94079, 1090 GB Amsterdam, the Netherlands (s.dubinkina@cwi.nl). Supported by the Research Council for Earth and Life Sciences (ALW) with financial aid from the Netherlands Organization for Scientific Research (NWO).

†Centrum Wiskunde & Informatica, P.O. Box 94079, 1090 GB Amsterdam, the Netherlands (jason@cwi.nl).

‡School of Mathematics and Maxwell Institute for Mathematical Sciences, The University of Edinburgh, James Clerk Maxwell Building, The King's Buildings, Mayfield Road, Edinburgh, Scotland EH9 3JZ (b.leimkuhler@ed.ac.uk).

in which a system of particles is in thermal equilibrium with a reservoir. This point of view has been exploited by Bühler [2] in a numerical/statistical investigation of the work of Onsager [13], and our goal here is to reproduce the results of [2] without explicitly accounting for the individual motions of the reservoir of small vortices.

A thermostat is a tool used in molecular dynamics to model a system in thermal equilibrium with a reservoir; such thermostats may be either stochastic (e.g. Langevin dynamics) or deterministic. In a Langevin dynamics simulation a stochastic perturbation is introduced in the force field together with a dissipative term; these terms are maintained in balance so as to preserve the canonical ensemble. With a dynamical (or deterministic) thermostat, by contrast, the system is augmented by a few degrees of freedom that model the exchange with the reservoir. The goal of thermostating is to force the system to sample the canonical equilibrium distribution at a given temperature by continually perturbing it. A benefit of the dynamical models is that it is possible to conserve structure (e.g. Hamiltonian structure) in the augmented dynamics. A motivation for using this approach is that if the perturbation is small, the dynamics will still correspond to physical dynamics (in contact with a reservoir) on an intermediate timescale. Some examples of important deterministic thermostating methods are the Nosé method [10, 11], which preserves Hamiltonian structure at the expense of a continuous rescaling of time, the Nosé-Hoover method [11, 5] which recovers the linear time but loses canonical Hamiltonian structure, the Nosé-Poincaré method of Bond, Laird & Leimkuhler [1] which is canonically Hamiltonian, and a generalization of the Nosé-Hoover approach for Hamiltonian systems with Poission structure [3]. Deterministic thermostats have also been coupled with Langevin models in [9] for example.

In this paper we propose the use of a thermostat to model the unresolved vorticity and its exchange in a simple point vortex model. We will model both an infinite reservoir as in classical thermodynamics, and a finite reservoir as has been used in the experiments of [2]. Statistics of the thermostated dynamics will be compared with the results of Bühler [2]. In §2 we make use of a generalized thermostat which can be used to force a Hamiltonian system to sample a general class of equilibrium distributions. The point vortex model and its statistical mechanics is reviewed in §3. In §4 we present the details of the thermostated numerical methods considered, including the models for finite and infinite reservoirs. Finally, in §5 the numerical schemes are verified by comparison with results from the literature.

2. Generalized thermostats. Consider an open subset $\mathcal{D} \subset \mathbb{R}^d$ and a deterministic differential equation

$$\dot{X} = f(X), \qquad X(t) \in \mathcal{D}, \qquad f : \mathcal{D} \to \mathbb{R}^d. \tag{2.1}$$

A probability distribution $\rho(X,t) \in \mathcal{D} \times \mathbb{R} \to \mathbb{R}$, $\rho \geq 0$, on $\mathcal{D}$ is transported under the vector field f according to the continuity equation

$$\frac{\partial}{\partial t}\rho(X,t) + \nabla \cdot \rho(X,t) f(X) = 0. \tag{2.2}$$

This continuity equation implies that $\int_{\mathcal{D}} \rho \, dX = 1$ for all $t > 0$ if this holds at $t = 0$. An equilibrium distribution is a stationary solution of (2.2). In this paper we will be concerned primarily with systems of the form

$$\dot{X} = J(X)\nabla H(X), \qquad X(t) \in \mathcal{D}, \quad J^T = -J, \quad H : \mathcal{D} \to \mathbb{R}. \tag{2.3}$$

The function H is a first integral of (2.3), typically the energy. If J is independent of X, then this defines a (generalized) Hamiltonian system. Otherwise, one must also show that $J(X)$ satisfies the Jacobi identity, in which case the system is Poisson. We make the weaker assumption that the vector field on the right side of (2.3) is divergence-free, i.e. $\nabla \cdot f(X) \equiv 0$, so that the transport equation (2.2) simplifies to the Liouville equation

$$\frac{d}{dt}\rho(X,t) = \frac{\partial}{\partial t}\rho(X,t) + f(X)\cdot\nabla\rho(X,t) = 0. \tag{2.4}$$

An equilibrium distribution $\frac{\partial \rho}{\partial t} \equiv 0$ must satisfy

$$f(X)\cdot\nabla\rho(X) \equiv 0.$$

Note that any function $\rho(X) = \rho(H(X))$ that depends on X through a first integral is an equilibrium distribution. If (2.1) has additional first integrals $I_2(X), \ldots, I_p(X)$, then any distribution $\rho(H, I_2, \ldots, I_p)$ is also an equilibrium distribution. The ensemble average of a function $F(X)$ with respect to the equilibrium distribution $\rho(X)$ is

$$\langle F\rangle := \int_{\mathcal{D}} F(X)\rho(X)\,dX.$$

Given their ample supply, the degree to which a given equilibrium distribution is meaningful largely depends on whether the solution to the differential equation is ergodic in that distribution such that the long time average of any function $F(X(t))$ of the solution

$$\overline{F} := \lim_{T\to\infty}\frac{1}{T}\int_0^T F(X(t))\,dt,$$

converges to the ensemble average in the distribution, i.e. satisfies

$$\overline{F} = \langle F\rangle$$

for almost any solution trajectory. If this is the case, the equilibrium distribution characterizes the long time behavior of solutions of the differential equation.

The microcanonical ensemble [7] applies to an isolated system at constant energy, and is the singular measure on the energy level set containing the initial condition

$$\rho_\mu \propto \delta(H(X) - H_0), \tag{2.5}$$

where $H_0 = H(X(0))$. This ensemble is appropriate for a numerical simulation with an energy conserving discretization.

A system in contact with a large reservoir does not conserve energy, but rather exchanges it with the reservoir. If it is in thermal equilibrium with a reservoir of statistical temperature β^{-1}, then the appropriate ensemble is the canonical ensemble [7] with Gibbs measure

$$\rho(X) = Z^{-1}\exp(-\beta H(X)), \tag{2.6}$$

where $Z = \int_{\mathcal{D}}\exp(-\beta H(X))\,dX$. It is clear, however, that a single solution of the system (2.3) will not be ergodic in the Gibbs measure, since with probability one it

will sample the constant energy surface containing the initial condition, whereas (2.6) assigns nonzero probability to all energy surfaces. Instead, to model a system in thermal equilibrium with a reservoir, one must devise a method whose dynamics samples phase space with probability given by the canonical distribution (2.6). The development of methods that do just this constitutes an active field of research. A number of techniques have been developed for sampling in a given distribution, including Monte Carlo schemes, which generate random configurations or trajectories according to the chosen distribution; Langevin thermostats, in which the original system of ordinary differential equations is augmented by stochastic forcing and generalized dissipation terms; and deterministic thermostats, in which the reservoir itself is modelled using a small number of additional degrees of freedom. The latter approaches have the advantage that they generate plausible solution behavior, and can be used to compute correlations.

In the next two sections we describe generalized Langevin dynamics and generalized stochastic Bulgac-Kusnezov thermostats for sampling in a wide class of equilibrium distributions for Hamiltonian systems.

2.1. Langevin thermostat. If one integrates (2.3) numerically using a symplectic integrator, the Hamiltonian will typically be well-conserved. As a result, the solution will not sample phase space with the measure (2.6) above, but instead will stay near the initial energy level set (at best sampling ρ_μ). For some applications it is desirable to construct a perturbed dynamical system that does sample ρ while retaining something of the dynamical behavior of (2.3). In this way one can construct a plausible (representative) behavior of the system if it were exchanging energy with the reservoir according to ρ.

One approach to sample a given equilibrium distribution augments (2.3) with carefully tuned noise and dissipation terms:

$$\dot{X} = f(X) + g(X) + \Sigma(X)\dot{w}(t), \tag{2.7}$$

where $g(X) : \mathcal{D} \to \mathbb{R}^d$, $\Sigma(X) \in \mathbb{R}^{d\times d}$ is a matrix valued function, and $w(t)$ is a vector Wiener process, i.e. the $w_i(t)$, $i = 1, \ldots, d$, are scalar Gaussian random variables with mean zero and increments $w_i(t) - w_i(s) \sim \mathcal{N}(0, t - s)$. Phase space densities are transported by the flow of (2.7) according to the Fokker-Planck equation (see, for example [14])

$$\frac{\partial}{\partial t}\rho(X,t) = -\nabla\cdot\rho(X,t)(f(X)+g(X)) + \frac{1}{2}\nabla\cdot\nabla\cdot\rho(X,t)\Sigma(X)\Sigma^T(X), \tag{2.8}$$

where $g(X)$ must be determined such that the desired equilibrium distribution is a stationary solution of (2.8). If ρ depends on X only through its Hamiltonian $\rho(X) = \rho(H(X))$, then the Hamiltonian dynamics drops out of the Fokker-Planck equation, since

$$\nabla\cdot\rho(H(X))J\nabla H(X) = \rho\nabla\cdot J\nabla H - \rho\nabla H\cdot J\nabla H = 0$$

by the divergence free nature of the Hamiltonian flow and conservation of energy. The Fokker-Planck equation reduces to

$$\frac{\partial}{\partial t}\rho(X,t) = -\nabla\cdot\rho(X,t)g(X) + \frac{1}{2}\nabla\cdot\nabla\cdot\rho(X,t)\Sigma(X)\Sigma^T(X).$$

The right hand side is zero if

$$-\rho(X)g(X) + \frac{1}{2}\nabla\cdot\rho(X)\Sigma(X)\Sigma^T(X) = 0.$$

For the canonical equilibrium distribution (2.6), we can solve this for $g(X)$ (suppressing the dependence on X in the notation):

$$\rho g(X) = \frac{1}{2}\rho\nabla\cdot\Sigma\Sigma^T - \frac{1}{2}\beta\rho\Sigma\Sigma^T\nabla H = \rho\left(\frac{1}{2}\nabla\cdot\Sigma\Sigma^T - \frac{1}{2}\beta\Sigma\Sigma^T\nabla H\right).$$

For $\Sigma(X)$ constant, this becomes

$$g(X) = -\frac{1}{2}\beta\Sigma\Sigma^T\nabla H(X).$$

Hence, the Langevin dynamics is

$$\dot{X} = J\nabla H(X) - \frac{\beta}{2}\Sigma\Sigma^T\nabla H(X) + \Sigma\dot{w}. \tag{2.9}$$

If the flow map is in addition ergodic with respect to ρ, then the generalized Langevin dynamics (2.7) can be used to sample the canonical distribution at inverse temperature β.

Remark. For $\Sigma = \Sigma(X)$ locally defined the noise is multiplicative, one must specify whether the Itô or Stratanovich interpretation is used, and numerical methods must be carefully constructed to maintain accuracy.

2.2. A generalized Bulgac-Kusnezov method. The following approach generalizes the Bulgac-Kusnezov method [3] and offers additional flexibility. The method has been proposed for canonical sampling in the molecular dynamics setting in [8]; here we treat an arbitrary smooth ensemble and apply it to the fluid vortex model. We introduce a new variable $\zeta \in \mathbb{R}$ and functions $s(X,\zeta) : \mathcal{D}\times\mathbb{R} \to \mathbb{R}^d$ and $h(X,\zeta) : \mathcal{D}\times\mathbb{R}\to\mathbb{R}$ and form the coupled system

$$\dot{X} = J\nabla H(X) + s(X,\zeta), \tag{2.10}$$

$$\dot{\zeta} = h(X,\zeta). \tag{2.11}$$

We ask that the following extended measure be invariant under the Liouville equation:

$$\tilde{\rho}(X,\zeta) \propto \exp(-\beta F(X) - \alpha G(\zeta)) \tag{2.12}$$

for F and G appropriately defined functions. In the case of (2.6) we will take $F \equiv H$, but we consider this more general formulation for now. Note that after integration over ζ, this measure is of the form (2.6). The stationarity condition for the transport equation (2.2) is

$$\nabla\cdot\tilde{\rho}\,(f+s) + \partial_\zeta(\tilde{\rho}h) = 0, \quad \text{with } f = J\nabla H(X).$$

Some calculations give

$$\begin{aligned}
0 &= (f+s)\cdot\nabla\tilde{\rho} + \tilde{\rho}\nabla\cdot(f+s) + h\frac{\partial}{\partial\zeta}\tilde{\rho} + \tilde{\rho}\frac{\partial}{\partial\zeta}h \\
&= -\beta\tilde{\rho}\nabla F\cdot(f+s) + \tilde{\rho}\nabla\cdot(f+s) - \alpha\tilde{\rho}h\frac{\partial}{\partial\zeta}G + \tilde{\rho}\frac{\partial}{\partial\zeta}h \\
&= \tilde{\rho}(-\beta\nabla F\cdot(f+s) + \nabla\cdot s - \alpha h\frac{\partial}{\partial\zeta}G + \frac{\partial}{\partial\zeta}h),
\end{aligned}$$

where the divergence-freedom of the Hamiltonian vector field is used in the last inequality.

Next we make some simplifying assumptions. First we assume the thermostat variable ζ to be normally distributed, taking $G(\zeta) = \zeta^2/2$. We also assume that h depends only on X, i.e. $h(X,\zeta) = h(X)$. The stationarity condition consequently reduces to

$$0 = -\beta \nabla F \cdot (f+s) + \nabla \cdot s - \alpha h \zeta.$$

We wish to use this relation to define h. Note that

$$\zeta h(X) = \frac{1}{\alpha}\left(\nabla \cdot s - \beta \nabla F \cdot (f+s)\right). \tag{2.13}$$

Since ζ may be zero, each term on the right should either vanish or have precisely a factor ζ as on the left. Candidate equilibrium distributions for (2.3) typically have functional dependence via the Hamiltonian. If we assume $F(X) := F(H(X))$, then the skew-symmetry of J implies

$$\nabla F \cdot f = F'(H(X)) \nabla H \cdot J \nabla H \equiv 0.$$

If additionally we assume $s(X,\zeta)$ to be linear in ζ, i.e.

$$s(X,\zeta) = s_1(X)\zeta, \qquad s_1(X) \in \mathbb{R}^d,$$

then we find that

$$h(X) = \frac{1}{\alpha}\left(\nabla \cdot s_1(X) - \beta \nabla F \cdot s_1(X)\right) \tag{2.14}$$

is a solution of (2.13).

Specific choices of the functions $F(X)$ and $s_1(X)$ will be treated in Section 4.

In general, the thermostated dynamics so defined will not be ergodic in the invariant measure (2.12). To improve ergodicity, a Langevin term may be added to (2.11). See also [9].

$$\dot{X} = J\nabla H(X) + s_1(X)\zeta, \tag{2.15}$$

$$\dot{\zeta} = h(X) - \frac{\alpha\sigma^2}{2}\zeta + \sigma\dot{w}. \tag{2.16}$$

Since the noise enters through ζ, it influences $X(t)$ only after integration, so its effect on the dynamics is smoothed.

Remark. In the important special case $F(X) := F(H(X))$, if we choose s_1 such that $\nabla \cdot s_1 \equiv 0$, then the system (2.15)-(2.16) can be cast in the form of a generalized Langevin thermostat (2.9) as discussed in the previous section. Define the augmented system

$$\tilde{X} = \begin{pmatrix} X \\ \zeta \end{pmatrix}, \qquad \tilde{J}(\tilde{X}) = \begin{bmatrix} \frac{1}{F_H} J & \frac{\beta}{\alpha} s_1(X) \\ -\frac{\beta}{\alpha} s_1(X)^T & 0 \end{bmatrix}, \qquad \tilde{H}(X,\zeta) = F(H(X)) + \frac{\alpha}{2\beta}\zeta^2. \tag{2.17}$$

Then (2.15)-(2.16) with (2.14) takes the form

$$\frac{d}{dt}\tilde{y} = \tilde{J}\nabla\tilde{H} - \frac{\alpha}{2}\Sigma\Sigma^T\nabla\tilde{H}(\tilde{X}) + \Sigma\dot{w} \tag{2.18}$$

with $\Sigma = \left[\begin{smallmatrix} 0 \\ \sigma \end{smallmatrix}\right]$.

3. Statistical mechanics of point vortices. The motion of N point vortices with circulation strengths $\Gamma_i \in \mathbb{R}$, $i = 1, \ldots, N$, and positions $x_i(t) \in \mathbb{R}^2$ is given by the Hamiltonian system

$$\Gamma_i \dot{x}_i = K \frac{\partial H}{\partial x_i}, \qquad i = 1, \ldots, N, \tag{3.1}$$

where $K = \left(\begin{smallmatrix} 0 & 1 \\ -1 & 0 \end{smallmatrix}\right)$, and the Hamiltonian

$$H = -\frac{1}{4\pi} \sum_{i<j} \Gamma_i \Gamma_j \ln(|x_i - x_j|^2)$$

represents the kinetic energy.

If there are Γ_i with both positive and negative circulations, then the motion of point vortices is unbounded on the plane. A bounded flow can be ensured by imposing periodicity, which alters the Green's function in the Hamiltonian [16]. Alternatively, flow on a disc of radius R can me modeled by defining a set of image vortices

$$\Gamma_i' = -\Gamma_i, \quad x_i' = x_i \frac{R^2}{|x_i|^2}, \quad i = 1, \ldots, N$$

which ensure that the velocity field observed by any point vortex is tangent to the wall. In the disc model, which we adopt in this paper, the Hamiltonian has three terms due to: the original pair potential, the self-interaction, and the interaction terms of each vortex with the images of the others:

$$\begin{aligned} H = -\frac{1}{4\pi} \sum_{i<j} \Gamma_i \Gamma_j \ln(|x_i - x_j|^2) + \frac{1}{4\pi} \sum_i \Gamma_i^2 \ln(R^2 - |x_i|^2) + \\ \frac{1}{4\pi} \sum_{i<j} \Gamma_i \Gamma_j \ln(R^4 - 2R^2 x_i \cdot x_j + |x_i|^2 |x_j|^2). \end{aligned} \tag{3.2}$$

To cast the system (3.1) in the form (2.3), we define $X = (x_1^T, \cdots, x_N^T)^T$, $H = H(X)$, and

$$J = \begin{bmatrix} \Gamma_1^{-1} K & & \\ & \ddots & \\ & & \Gamma_N^{-1} K \end{bmatrix}.$$

Besides the kinetic energy, the point vortex flow on the disc conserves the total angular momentum, defined as

$$M = \frac{1}{2\pi} \sum_i \Gamma_i |x_i|^2. \tag{3.3}$$

In general there will be an exchange of momentum between the strong vortices and the reservoir. However on average we would expect the angular momentum of both strong and weak vortex sets to be approximately constant. In fact, it would be straightforward to model the exchange of angular momentum using the thermostat as well. This would require knowledge of the variance of the angular momentum of the reservoir. In this paper we assume the momentum exchange with the reservoir is negligible, and

we can show that M is a conserved quantity of the thermostated dynamics. Experiments with Langevin dynamics indicate significant drift in angular momentum. To correct this, one could construct a projection of the noise term $\Sigma(X)$ onto the angular momentum manifold. However, this comes at the cost of multiplicative noise.

The phase space of the point vortex flow consists of the direct product of N copies of the domain. If the domain is bounded, so is the phase space. The energy H is unbounded on the phase space however: as $x_i \to x_j$, the logarithm tends to $-\infty$; if Γ_i and Γ_j are like-signed, $H \to +\infty$, if oppositely-signed, $H \to -\infty$. In particular, if a particle collides with the wall, $H \to -\infty$. As noted by Onsager [13], if we define $\Omega(E)$ to be the measure of the set of configurations in phase space for which $H \in (E, E + dE)$, then we must have $\lim_{E\to\pm\infty} \Omega(E) = 0$. In other words, since the phase space is bounded, the measure of available phase space must eventually decrease as an increasing function of energy. The situation is in contrast to other n-body problems encountered in chemistry and astronomy, where the positive definite kinetic energy terms can accommodate any amount of energy, and the measure of available phase space is a monotone increasing function of energy.

Consequently, the microcanonical entropy $S(E) = \ln \Omega(E)$ must attain a maximum for some E^*. The microcanonical temperature is defined to be $T_\mu^{-1} = \frac{d}{dE} \ln S(E)$. As temperature varies from $-\infty$ to ∞ along the real line, the associated energy states vary from $E > E^*$ to $E < E^*$ through infinity. In other words temperature passes through zero via a collision. This has important consequences for thermostating, since it implies that that the vortices will collapse to the wall if the temperature changes sign continuously.

Recall that extreme values of the energy H are associated with close approaches between vortices or image-vortices. As noted by Bühler [2], for a homogeneous system with $\Gamma_i = \Gamma$, the energy largely governs the dynamics, since collisions have to occur roughly at constant energy. The situation is more interesting in a heterogeneous system with vortices of greatly differing strength. Onsager predicted that for such systems, extreme values of energy would increase the probability of clustering of like-signed or opposite-signed vortices, with a preference for the strongest ones, such that most of the energy would reside in a few degrees of freedom. As a result, the small vortices would roam aimlessly about, not developing into coherent structures, but exhibiting large entropy.

Bühler discusses Onsager's ideas in the context of the canonical ensemble applied to the strong vortices, which constitute a system in 'thermal' equilibrium with the reservoir of weak vortices. He verifies Onsager's predictions using numerical experiments with a system of 100 point vortices, four having strength $\pm 10\pi$ and the rest having strength $\pm 2\pi$. In each group, half the vortices had positive circulation and half negative. Experiments were carried out for extreme positive, neutral and extreme negative inverse statistical temperatures $\beta_\mu = T_\mu^{-1}$ in the microcanonical sense. In each case the strong vortices had the same (nearly steady state) initial configuration, so the differences in energy were only due to the random placement of weak vortices. Simulations were run on a long time interval, and statistics were recorded for the distance between like and opposite signed strong vortices, distance from the wall, and energy in the strong vortices. Bühler distinguishes between a theoretical infinite reservoir and the finite reservoir comprised of the 96 weak vortices. In the infinite reservoir case, the canonical probability measure only exists for a finite interval of inverse temperature β, whose boundary corresponds to collisions. This situation is due to the availability of an infinite amount of energy in the reservoir, and has impli-

cations for thermostating in the canonical ensemble. Specifically, if one thermostats in the canonical ensemble and increases β beyond its admissible range, the vortices will collapse onto the boundary. Bühler also points out that the contact with a finite reservoir will suppress this collapse, allowing thermostating at all temperatures. This is because there is a finite amount of energy in the finite reservoir, and this effectively bounds the closeness of approach of any two vortices from below. The probability of a close approach becomes very small. The probability of $H = E$ for a system in contact with a finite reservoir decays like $\exp(-\gamma E^2)$ with E for some $\gamma > 0$.

4. A thermostated integrator for point vortices. Our goal is to apply the generalized Bulgac-Kusnezov thermostat from §2.2 to the point vortex flow of §3. In this section we fill in the details of the method. First, in §4.1 we specify two equilibrium distributions corresponding to the cases where the reservoir of small scale vorticity is finite or infinite. In §4.2 we define a thermostat function s_1 such that the generalized Bulgac-Kusnezov thermostat is a Langevin thermostat. We describe the numerical method used to integrate the model adaptively in time in §4.3 and the means of computing the temperature in §4.4.

4.1. Infinite and finite reservoir ensembles. As discussed in [2] the behavior of a thermostated point vortex system can vary considerably depending on whether the reservoir is finite or infinite. In the case of an infinite reservoir, as the temperature of the reservoir is pushed toward zero, the subsystem may draw an arbitrarily large amount of energy from the reservoir, leading to collisions between individual vortices or with the wall. For a finite reservoir, there is a limited amount of energy available such that a collision may only occur if a collision with opposite energy occurs at the same time, and this is improbable. Specifically, in the case of a finite reservoir with normally distributed reservoir energy, the equilibrium distribution takes the form

$$\tilde{\rho}(X) = \exp\left(-\beta H(X) - \gamma H(X)^2\right).$$

For the generalized thermostat (2.10)–(2.11) we can model both finite and infinite reservoirs. For a finite reservoir we take

$$F(X) := H(X) + \frac{\gamma}{\beta} H(X)^2, \qquad h(X) = \frac{1}{\alpha}\left(\nabla \cdot s_1(X) - (\beta + 2\gamma H(X))\nabla H \cdot s_1(X)\right), \tag{4.1}$$

and for an infinite reservoir $\gamma \equiv 0$ in the expressions above.

4.2. Choice of s_1. We make the following choice for the function s_1 in (2.14):

$$s_1(X) = -\begin{pmatrix} \frac{Kx_1}{|x_1|} \\ \vdots \\ \frac{Kx_N}{|x_N|} \end{pmatrix}. \tag{4.2}$$

The flow of the vector field s_1 preserves the distance of each point vortex from the center of the domain. Consequently the thermostated system (2.15)-(2.16) preserves the angular momentum (3.3).

Furthermore, this choice of s_1 is divergence-free:

$$\nabla \cdot s_1(X) \equiv 0,$$

implying that the thermostated dynamics is a generalized Langevin system (2.18), and that the integral $\tilde{H}$ in (2.17) with $F(H(X))$ from (4.1) is preserved in the limit $\sigma \to 0$ of zero noise and dissipation.

4.3. Implementation details. In our numerical implementation, time stepping was done using a splitting approach. We solved alternately the deterministic thermostat system and the stochastic equation for the thermostat variable. The deterministic system is solved with the implicit midpoint rule

$$\frac{X^{n+1} - X^n}{\tau} = J\nabla H(\hat{X}) - s_1(\hat{X})\hat{\zeta}, \tag{4.3}$$

$$\frac{\zeta^{n+1} - \zeta^n}{\tau} = h(\hat{X}), \tag{4.4}$$

where $\hat{X} = (X^{n+1} + X^n)/2$ and $\hat{\zeta} = (\zeta^{n+1} + \zeta^n)/2$.

The remaining vector field is an Ornstein-Uhlenbeck equation

$$\dot{\zeta} = -\frac{\alpha\sigma^2}{2}\zeta + \sigma\dot{w}$$

with exact solution

$$\zeta^{n+1} = e^{-\varepsilon\tau}(z^n + \sigma\sqrt{\frac{e^{2\varepsilon\tau} - 1}{2\varepsilon}}\Delta w), \tag{4.5}$$

where $\varepsilon = \alpha\sigma^2/2$ and $\Delta w \sim \mathcal{N}(0, 1)$. A full time step of size Δt is constructed by solving (4.5) with $\tau = \Delta t/2$ composed with (4.3)–(4.4) with $\tau = \Delta t$ composed with a second solution of (4.5), $\tau = \Delta t/2$.

During a close approach of two vortices, equivalently when the strong vortex energy is large in magnitude, accuracy and stability considerations motivate the use of an adaptive time-stepping strategy. Given a stepsize Δt_n in the nth time step, the subsequent time step is found by solving

$$\Delta t_n \Delta t_{n+1} = \ell(X^n)^2 \Delta s^2. \tag{4.6}$$

Here, Δs is a uniform timestep under the time transformation $t = \ell \cdot s$, and ℓ is a monitor function that measures the stiffness of the local solution. This adaptivity approach is explicit and time-reversible whenever the numerical integrator is symmetric. For our experiments we use

$$\ell(x) = \min_{i \neq j} |x_i - x_j|,$$

where the minimization is over all vortices and image vortices.

4.4. Computation of temperatures. We check the inverse temperature β and reservoir variance γ numerically assuming ergodicity. For some function $a(X) : \mathcal{D} \to \mathbb{R}^d$ and an equilibrium distribution $\rho(X) = \exp\left(-\beta^* \tilde{H}(X)\right)$

$$\nabla \cdot \rho(X)a(X) = a(X) \cdot \nabla\rho(X) + \rho(X)\nabla \cdot a(X) = -\beta^*\rho(X)a(X) \cdot \nabla\tilde{H} + \rho(X)\nabla \cdot a(X).$$

Formally integrating over phase space

$$\int_{\mathcal{D}} \nabla \cdot \rho(X)a(X)dX = -\beta^* \int_{\mathcal{D}} \rho(X)a(X) \cdot \nabla\tilde{H}\, dX + \int_{\mathcal{D}} \rho(X)\nabla \cdot a(X)dX. \tag{4.7}$$

The expression on the left is zero if either ρ or a is zero on the boundary $\partial\mathcal{D}$ of phase space. The boundary of $\mathcal{D}$ consists of configurations for which at least one point vortex

is located on the boundary of the disc. Such a configuration has energy $H \to -\infty$. Likewise, there are points in phase space where two or more point vortices collide and the Hamiltonian tends to $\pm\infty$. The Gibbs distribution (2.6) can be normalized only for β on an open interval [2]:

$$\beta \in \left(\frac{-8\pi}{\Gamma^2 N}, \frac{+4\pi}{\Gamma^2} \right). \tag{4.8}$$

To carry out the integration (4.7), we choose a for the form:

$$a = b/\rho, \qquad \rho(X) = \exp\left(-\beta H(X)\right),$$

where β is the desired inverse temperature and $b(X)$ is some function with $b = 0$ at the boundary of the phase space. In this case, the expression for β^* simplifies to

$$0 = -\beta^* \langle a \cdot \nabla \tilde{H} \rangle + \langle \nabla \cdot a \rangle.$$

If the flow is ergodic, then the ensemble averages can be replaced with time averages

$$\beta^* = \overline{\nabla \cdot a} / \overline{a \cdot \nabla \tilde{H}},$$

and the disagreement of β^* and β serves as a simple check for nonergodicity. For the infinite reservoir, $\tilde{H} = H$, and for the finite reservoir, $\tilde{H} = H + \gamma^*/\beta^* H^2$, yielding

$$0 = -\beta^* \langle a \cdot \nabla H \rangle - 2\gamma^* \langle a \cdot H \nabla H \rangle + \langle \nabla \cdot a \rangle.$$

Choosing two independent functions $a_1 = b_1/\rho$ and $a_2 = b_2/\rho$, where b_1 and b_2 are identically zero on $\partial\mathcal{D}$, these equations yield a linear system for β^* and γ^*. For our experiments we chose

$$b_1 = \nabla H \prod_i (R^2 - |x_i|^2)|x_i|^2, \quad b_2 = \nabla H \prod_i (R^2 - |x_i|^2)^2 |x_i|^4, \quad \rho = \exp(-\beta H - \gamma H^2),$$

where β is one of the three inverse temperatures (5.1) and γ is either 0 for the infinite reservoir or the corresponding reservoir variance (5.2) for the finite reservoir.

Figure 4.1 illustrates convergence of β^* to the values of β (5.1) for both the infinite and finite reservoir, as well as convergence of γ^* to γ (5.2) for the finite reservoir.

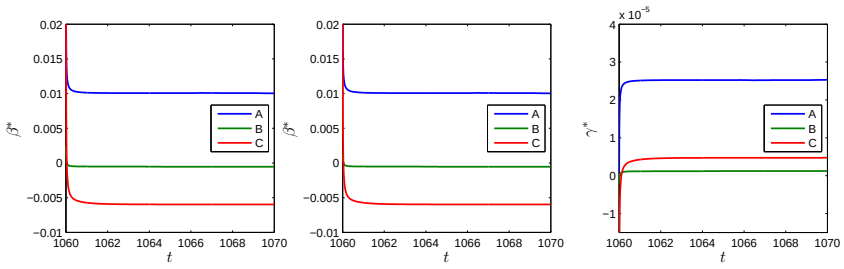

FIG. 4.1. *Convergence of inverse temperature β and reservoir variance γ for high (A), medium (B) and low (C) temperature states. Left: infinite reservoir β^*. Middle: finite reservoir β^*. Right: finite reservoir γ^*.*

5. Numerical experiments. For all of the numerical experiments using four strong vortices, the initial configuration consists of point vortices with circulations and positions given by [2]:

$$\Gamma_1 = \Gamma_3 = 10\pi, \qquad \Gamma_2 = \Gamma_4 = -10\pi,$$
$$x_1 = (3,0), \quad x_3 = (-3,0), \quad x_2 = (0,3), \quad x_4 = (0,-3).$$

For both the finite and infinite reservoir thermostat we choose negative, neutral and positive inverse temperatures

$$\beta = \{-0.006, -0.00055, 0.01\}. \tag{5.1}$$

Our choice of β is such that it is close to the theoretical upper limit in (4.8) for high temperature, and it is close to the theoretical lower limit in (4.8) for low temperature.

The size of the reservoir is defined by γ. In the case of an infinite reservoir $\gamma \equiv 0$, for a finite reservoir

$$\gamma = \beta/(-2E_0) \quad \text{with} \quad E_0 = \{628, 221, -197\}. \tag{5.2}$$

In all experiments, we take $\alpha = 0.5$ and $\sigma = \sqrt{0.4}$.

We integrated the thermostated dynamics over the interval $t \in [0, T]$ with $T = 12000$ using the time transformation (4.6) and fixed transformed time steps $\Delta s = \Delta t_0/\ell(X^0)$ with $\Delta t_0 = 0.001$. The sampling was performed over the time interval $[T_0, T]$ with $T_0 = 1500$, to allow decorrelation of the initial conditions. The resulting time series was sampled uniformly in time in cycles of $\delta t = 0.01$, to produce the histograms shown in Figures 5.5–5.8.

5.1. Ergodicity tests. The extended measure (2.12) is Gaussian in the thermostat variable ζ. If the time dynamics is ergodic with respect to (2.12), we expect the time series $\zeta(t)$ to be normally distributed, i.e. $\zeta \in \mathcal{N}(0, \alpha^{-1})$. A histogram of the values of ζ is shown in Figure 5.1 for the neutral case $\beta = -0.00055$. The normal distribution $\rho(\zeta) = \sqrt{\frac{\alpha}{2\pi}} \exp(-\frac{\alpha}{2}\zeta^2)$ is also plotted in the figure. The agreement is good, indicating ergodicity with respect to ζ.

As a second indication of ergodicity, we plot the motion of a single vortex $x_1(t)$ in Figure 5.2. The motion appears well-mixed. The density of points along the trajectory is greater where either the local velocity $\dot{x}_1$ or the local time step Δt_n is small.

5.2. Momentum conservation. The function $s_1(X)$ in (4.2) is chosen to preserve angular momentum (3.3) of the strong vortex set under the thermostated dynamics. Figure 5.3 shows the angular momentum M as a function of time for the three temperatures. We observe that M is preserved to the relative precision of the fixed point iteration used to solve (4.3)–(4.4).

5.3. Temperature effects. In this section we attempt to reproduce the experiments of Bühler using thermostated large point vortices. We conduct experiments using both the infinite reservoir canonical distribution ((4.1) with $\gamma \equiv 0$) and the finite reservoir distribution ((4.1) with $\gamma \neq 0$).

The time evolution of the kinetic energy of strong vortices is displayed in Figure 5.4 for both the infinite and finite reservoir models, showing that the thermostat drives the energy evolution towards the desired temperature. Figure 5.5 shows the probability distributions of the kinetic energy of the vortices. For the finite reservoir thermostat, the means and variances are similar to those of [2].

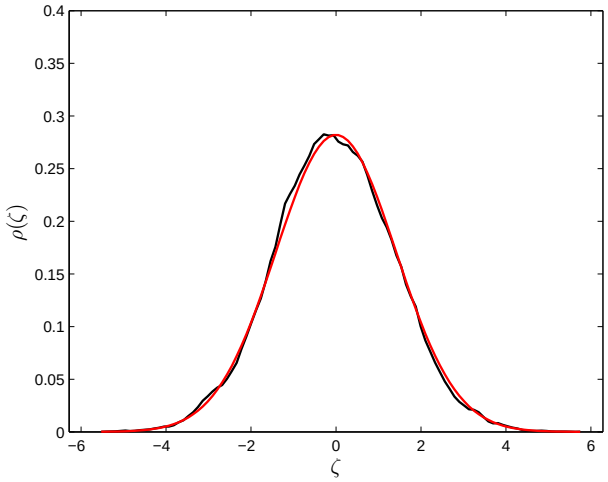

FIG. 5.1. *Distribution of thermostat (black line), Gaussian fit (red line).*

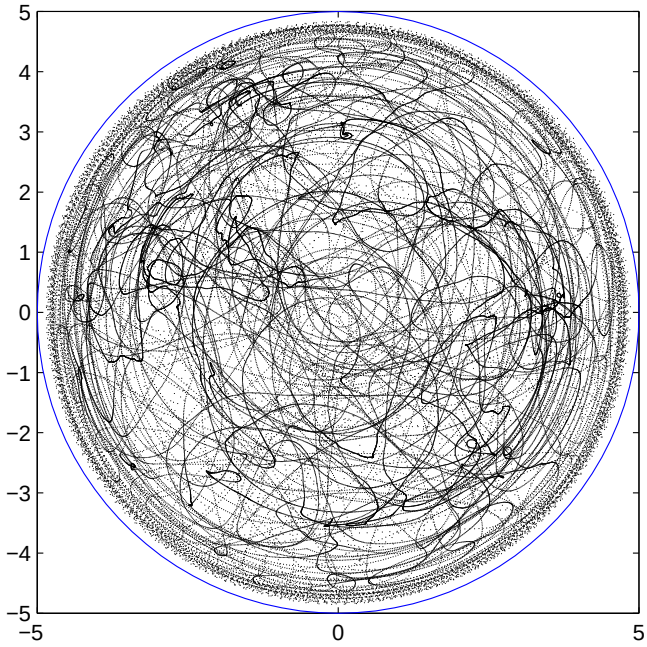

FIG. 5.2. *Motion of a single vortex $x_1(t)$ on the interval $t \in [0, 1000]$ for $\beta = -0.00055$.*

Figure 5.6 displays the histogram of distances $|x_i - x_j|$ between like-signed vortices. Bias in favor of small separations is evident at negative temperatures, consistent with Onsager's predictions. The distributions are very similar to those obtained by Bühler [2]. For the infinite reservoir model, there is a large peak in the distribution at

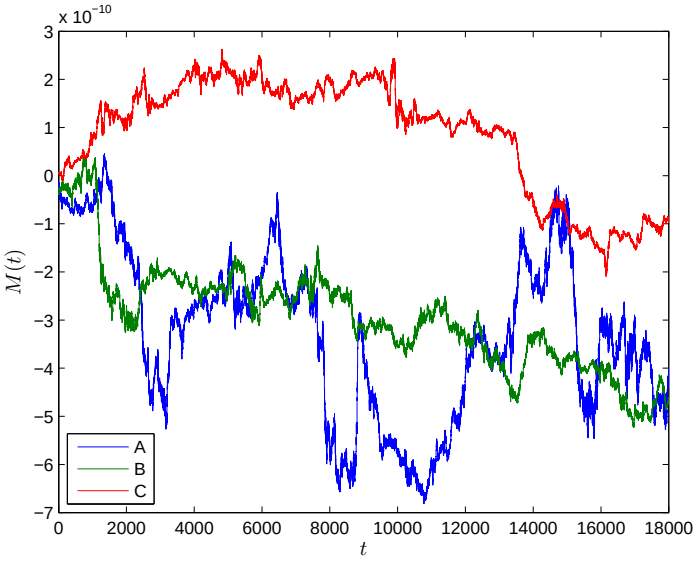

FIG. 5.3. *Momentum for high (A), medium (B) and low (C) temperature states for finite reservoir size. Infinite reservoir gives a similar behavior.*

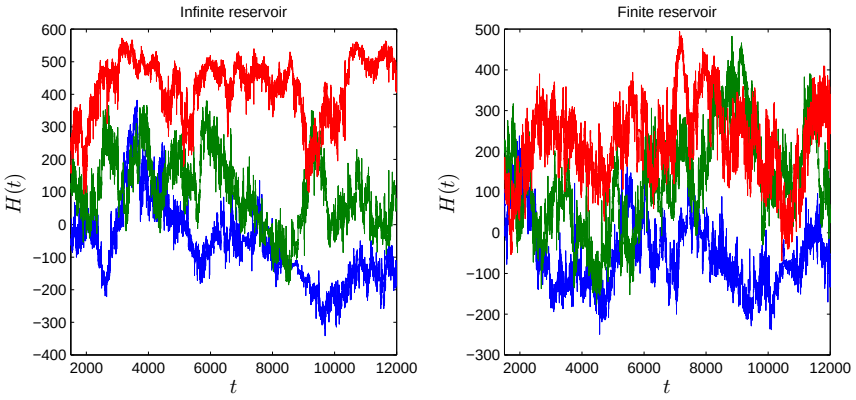

FIG. 5.4. *Time evolution of energy $H(t)$ for infinite (left) and finite (right) reservoirs. Inverse temperatures: $\beta = 0.01$ (blue), $\beta = -0.00055$ (green), $\beta = -0.006$ (red).*

$|x_i - x_j| \approx 1$ which is inconsistent with Bühler's simulations. This occurs because too much energy is drawn from the reservoir. The comparison is recovered in the finite reservoir model.

Figure 5.7 shows the histograms of the distance between opposite-signed vortices. In this case, there is a somewhat milder bias towards close approaches at negative temperatures, in keeping with Onsager's ideas. The bias is less pronounced because the close approaches between a point vortex and its opposite signed image across the domain boundary are not included in this statistic. Again the histograms are in excellent agreement with the simulation data of [2], for the finite reservoir simulation.

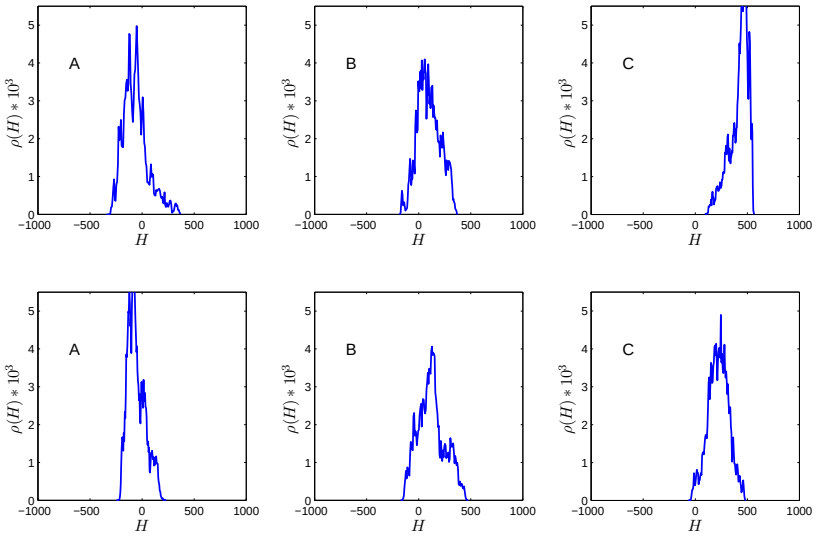

FIG. 5.5. *Distribution of energy for high (A), medium (B) and low (C) temperature states. Top: Infinite reservoir size. Bottom: Finite reservoir size.*

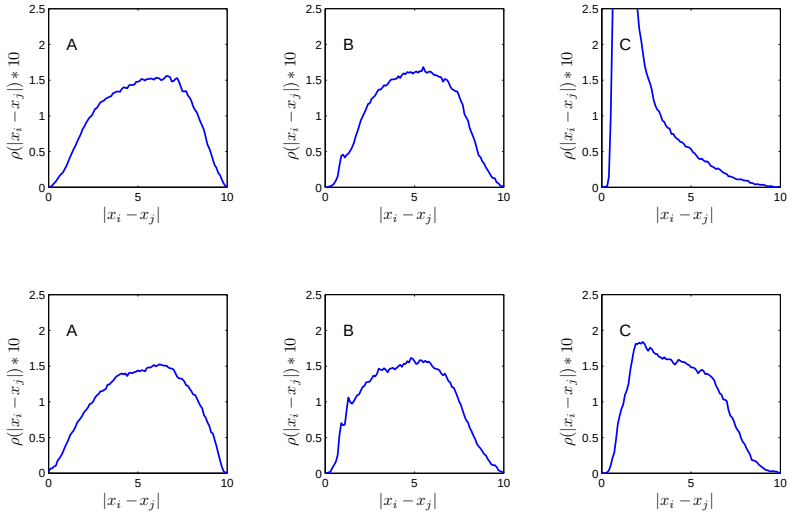

FIG. 5.6. *Interparticle spacing among same-signed vortices for high (A), medium (B) and low (C) temperature states. Top: Infinite reservoir size. Bottom: Finite reservoir size.*

For an infinite reservoir, the positive temperature histogram is more peaked.

Figure 5.8 shows histograms of the vortex distance from the origin. For positive temperature, the vortices accumulate near the wall. The finite reservoir figures are in excellent agreement with those of [2]. For the infinite reservoir, the peak at $|x_i| \approx 4.9$ is closer to the wall than for the finite reservoir, indicating that more energy is drawn from the reservoir in this case. At negative temperature, the vortices avoid the wall

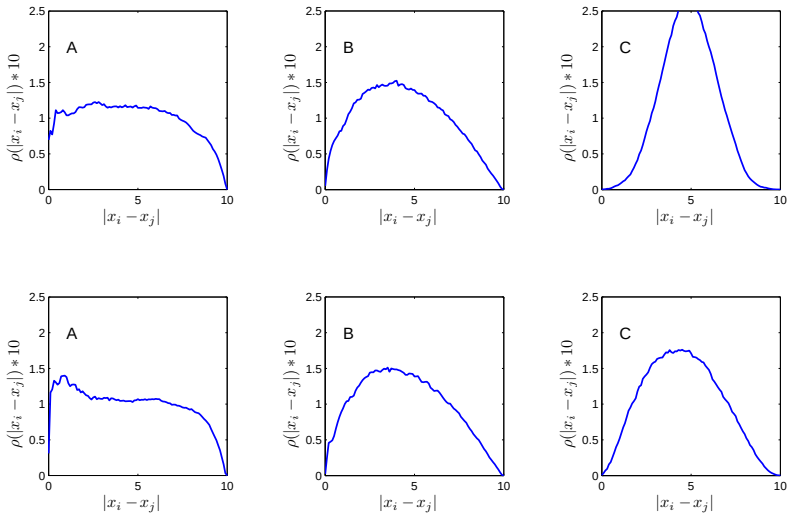

FIG. 5.7. *Interparticle spacing among opposite-signed vortices for high (A), medium (B) and low (C) temperature states. Top: Infinite reservoir size. Bottom: Finite reservoir size.*

with high probability.

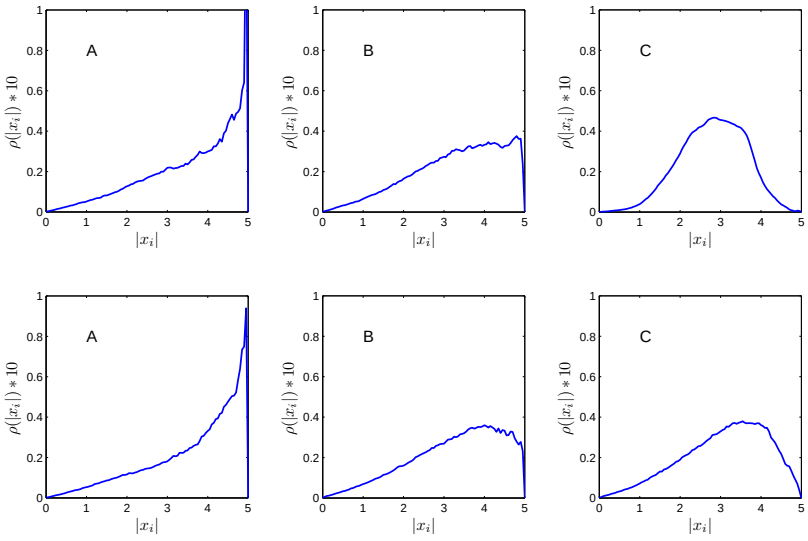

FIG. 5.8. *Distribution of distance from origin for high (A), medium (B) and low (C) temperature states. Top: Infinite reservoir size. Bottom: Finite reservoir size.*

To observe the effects of temperature on a larger collection of vortices, we also simulated a set of with $N = 12$, under the same conditions as above at the extremal temperatures $\beta = -0.006$ and $\beta = 0.01$. The initial positions in both cases were defined as shown in Figure 5.9 in the left panel. The middle and right panels of

Figure 5.9 show characteristic snapshots for each case. The linked animations illustrate the dynamics for positive and negative temperature regimes on a short interval $t \in [1500, 1500.1]$. At positive temperatures, vortices cluster in oppositely signed pairs, or translate parallel to the boundary of the domain. Because oppositely signed pairs translate normal to the dipole axis until they collide with another vortex or the boundary, these pairs are short lived. In contrast, for negative temperatures the vortices separate into two relatively stable regions of positive and negative circulation. Figure 5.10 shows a snapshot of the stream function from the positive and negative temperature simulations. For negative temperatures the vorticity is more concentrated in two counter-rotating patches. The linked animations illustrate the dynamics at positive (anim1.avi) and negative (anim2.avi) temperatures.

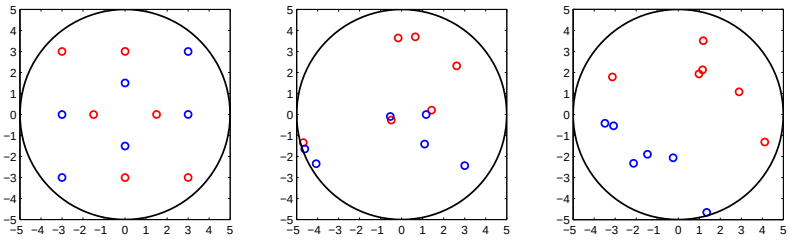

FIG. 5.9. *Snapshots of the case $N = 12$: the initial vortex placement (left), $\beta = 0.01$ (middle) and $\beta = -0.006$ (right). For positive temperature, clustering occurs pairwise; for negative temperature, large counter-rotating regions occur.*

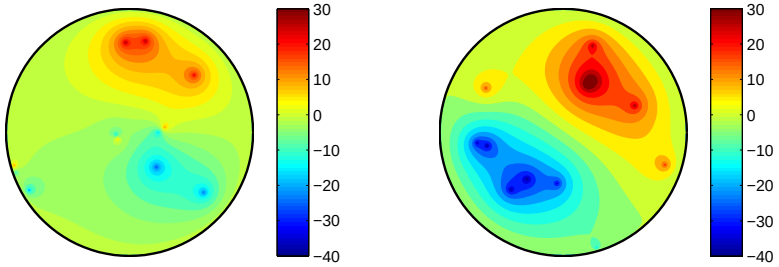

FIG. 5.10. *Snapshots of the stream function for case $N = 12$, $\beta = 0.01$ (left) and $\beta = -0.006$ (right). For negative temperature, clustering of like-signed vortices yields two strong counter-rotating vortices. See also linked animations* `anim1.avi` *($\beta = 0.01$) and* `anim2.avi` *($\beta = 0.006$).*

6. Conclusions. In this paper we provide proof of concept that the energy exchange between large scale point vortices with a reservoir of small scale point vortices can be well modeled with a simple thermostat device that adds only a single degree of freedom to the phase space of the large scale flow. Specifically, we are able to recover the canonical statistics of the strong vortices, as obtained from direct numerical simu-

lations in [2]. By constructing a thermostat for general energy-dependent equilibrium distributions, we model a canonical ensemble with a finite reservoir.

Acknowledgements. We express thanks to Jacques Vanneste for fruitful discussions during the early stages of this work.

REFERENCES

[1] Stephen D. Bond, Benedict J. Leimkuhler, and Brian B. Laird, *The Nosé-Poincaré method for constant temperature molecular dynamics*, J. Comput. Phys., 151 (1999), pp. 114–134. Computational molecular biophysics.
[2] Oliver Bühler, *Statistical mechanics of strong and weak point vortices in a cylinder*, Phys. Fluids, 14 (2002), pp. 2139–2149.
[3] A. Bulgac and D. Kusnezov, *Canonical ensemble averages from pseudomicrocanonical dynamics*, Phys. Rev. A, 42 (1990), pp. 5045–5048.
[4] Dale R. Durran, *Numerical methods for wave equations in geophysical fluid dynamics*, vol. 32 of Texts in Applied Mathematics, Springer-Verlag, New York, 1999.
[5] William G. Hoover, *Canonical dynamics: Equilibrium phase-space distributions*, Phys. Rev. A, 31 (1985), pp. 1695–1697.
[6] Willem Hundsdorfer and Jan Verwer, *Numerical solution of time-dependent advection-diffusion-reaction equations*, vol. 33 of Springer Series in Computational Mathematics, Springer-Verlag, Berlin, 2003.
[7] A.I. Khinchin, *Mathematical Foundations of Statistical Mechanics*, Dover, 1960.
[8] Benedict Leimkuhler, *Generalized Bulgac-Kusnezov methods for sampling of the Gibbs-Boltzmann measure*, In preparation, (2009).
[9] Benedict Leimkuhler, Emad Noorizadeh, and Florian Theil, *A gentle stochastic thermostat for molecular dynamics*, J. Stat. Phys., 135 (2009), pp. 261–277.
[10] Shuichi Nosé, *A molecular dynamics method for simulations in the canonical ensemble*, Mol. Phys., 52 (1984), pp. 255–268.
[11] ———, *A unified formulation of the constant temperature molecular dynamics methods*, J. Chem. Phys., 81 (1984), p. 511.
[12] Marcel Oliver and Oliver Bühler, *Transparent boundary conditions as dissipative subgrid closures for the spectral representation of scalar advection by shear flows*, J. Math. Phys., 48 (2007), pp. 065502, 26.
[13] L. Onsager, *Statistical hydrodynamics*, Nuovo Cimento (9), 6 (1949), pp. 279–287.
[14] G. A. Pavliotis and A. M. Stuart, *Multiscale Methods: Averaging and Homogenization*, Springer, New York, 2008.
[15] Rick Salmon, *Lectures on geophysical fluid dynamics*, Oxford University Press, New York, 1998.
[16] Jeffrey B. Weiss and James C. McWilliams, *Nonergodicity of point vortices*, Phys. Fluids A, 3 (1991), pp. 835–844.

Centrum Wiskunde & Informatica (CWI) is the national research institute for mathematics and computer science in the Netherlands. The institute's strategy is to concentrate research on four broad, societally relevant themes: earth and life sciences, the data explosion, societal logistics and software as service.

Centrum Wiskunde & Informatica (CWI) is het nationale onderzoeksinstituut op het gebied van wiskunde en informatica. De strategie van het instituut concentreert zich op vier maatschappelijk relevante onderzoeksthema's: aard- en levenswetenschappen, de data-explosie, maatschappelijke logistiek en software als service.

Bezoekadres:
Science Park 123
Amsterdam

Postadres:
Postbus 94079, 1090 GB Amsterdam
Telefoon 020 592 93 33
Fax 020 592 41 99
info@cwi.nl
www.cwi.nl

CWI

Centrum Wiskunde & Informatica